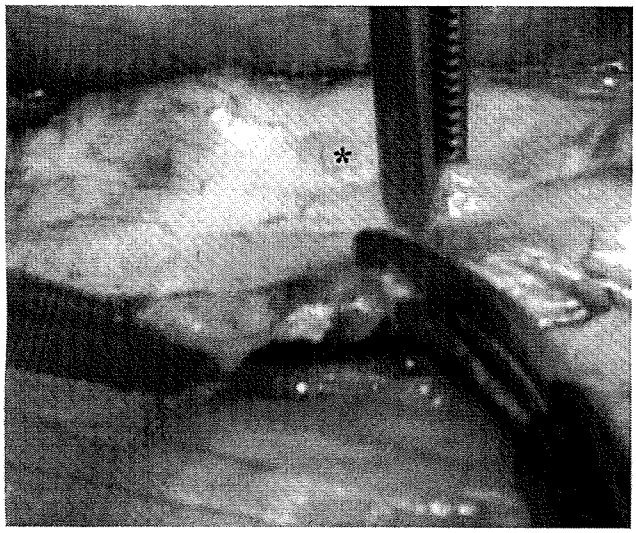

図 2　センチネルリンパ節の同定・摘出法
センチネルリンパ節は多方向に複数個存在することもあるので，胃周囲を広範囲に十分観察する必要がある。見つからないときは，出血しないように脂肪を切開しながらリンパ管を追跡することが重要で，小彎ではとくに注意を要する。図はピックアップ法によるものであり，小彎側に着色リンパ節を同定・摘出している。口側（画面奥の asterisk）には着色していないリンパ節が見える。

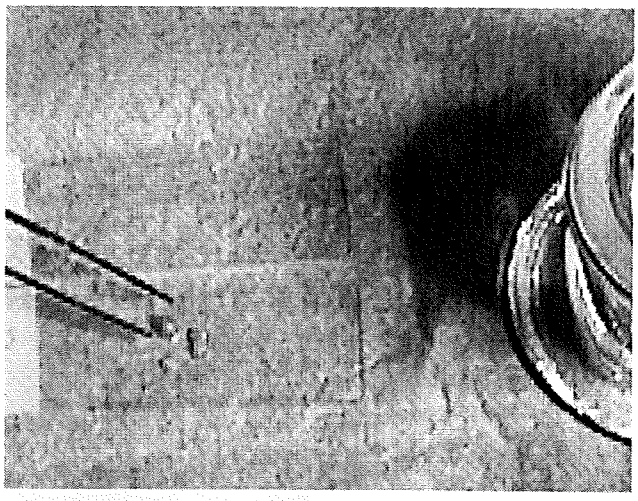

図 3　同定したセンチネルリンパ節の転移検索法
精度の高い術中迅速診断の観点から，通常の最大割面での組織診に加え，図のような多切片検索や捺印細胞診などが用いられているが，多施設共同研究においては，種々の制約から，最大割面1切片の HE 染色のみでの転移検索となっている。

精度の高い術中迅速診断が求められる。通常の最大割面での組織診に加え，多切片検索，捺印細胞診，免疫染色，分子生物学的診断などが用いられるが[7]（**図 3**），時間や人員の制約，分子生物学的手法では形態学的裏付けが取れないなどの問題がある。多施設共同研究でも，最大割面1切片（HE 染色）のみという制約が加わった。

SN 生検には病理部門の理解と協力が不可欠である。妥当性検証の現段階では郭清リンパ節すべての転移検索が要求され，SN 転移検索は作業を増やす要因となるが，将来的に SN 生検によりリンパ節郭清が省略されるようになれば，SN 以外のリンパ節に対する転移検索は必要なく，SN 転移検索に手間をかけたとしても，効率的といえる。

II.　胃癌に対するセンチネルリンパ節生検の手技

SN 診断の報告は症例数が限られ，方法も多種多様であり[6)8)10)]，SN concept の妥当性が十分検証されていないのが現状である。早期胃癌のリンパ節転移は少なく，SN 生検の妥当性検証には多数例での検討を要する。方法論を統一した多数例での多施設共同研究が必要との観点から，現在，日本臨床腫瘍研究グループ（Japan clinical oncology group，JCOG）と Sentinel node navigation surgery（SNNS）研究会による2つの多施設共同研究が行われている。両試験の検証点には違いがあり，SN 生検法も異なる。本稿では紙面の制約もあり，SN 生検の具体例として，両試験における手技を紹介することとする。

1. JCOG による多施設共同研究における手技

JCOG 胃がん外科グループによる多施設共同研究「早期胃癌におけるセンチネルリンパ節生検の妥当性に関する研究（JCOG0302）」（UMIN-CTR 試験 ID：C000000059）は，早期胃癌患者に対して，indocyanine green（ICG）を用いて同定された green node（GN）を SN とみなし，GN の術中迅速病理診断でリンパ節転移が陰性の場合にリンパ節郭清を行わないことが妥当であるかどうかを評価することを目的

とし，primary endpointは偽陰性割合（GN迅速病理診断転移陰性例／組織学的リンパ節転移陽性例）である。同意の得られた内視鏡的切除の対象とならない早期胃癌患者を対象とし，術中迅速組織診での妥当性評価である。たとえば，術中の迅速組織診で転移なしとされたGNの術後検索で転移を認めた場合，SN conceptとしては問題ないのだが，本試験では偽陰性と扱う。筆者らによるpilot studyでは多切片での転移検索を行っていたが[6]，多施設共同研究であるために最大割面1切片のHE染色のみでの検索という制約が加わっている。また，SN生検の手技慣れ期間が施設あたり5例と設定されているが，後述のSNNS研究会によるアンケート結果からすれば，ラーニングカーブが少なく見積もられている。すなわち，現時点での臨床応用が妥当であるかどうかを評価する臨床研究であるため，SN conceptの妥当性のみならず，術中迅速病理診断およびラーニングカーブの問題などが包含されている点に留意すべきである。

①開腹下に胃癌原発巣の視触診を行う。大網を胃大網動・静脈から十分離れた部位で切開して，胃の後面を観察できるようにする。原則として術前内視鏡下に病巣に接してクリップを付けておくが，病巣位置の確認に術中内視鏡を併用してもよい。

②肝機能検査と同様にICG 1バイアル25 mgを蒸留水5 mlに溶解する。色素の注入は胃の漿膜側から26ゲージ針を用いて行う。癌病巣に近接して，それを取り囲むように分注し，最低でも4 mlは注入する。

③色素注入後，5分経過してから緑色に着色したリンパ節の同定・摘出を開始する。緑色リンパ管を追跡しながらGNの検索を行う。通常約20分ですべてのGNの同定・摘出を終了することができるため，不必要に手術時間を延長させないよう，色素注入後30分を超えてのGNの同定を行わない。

④摘出したすべてのGNを最大割面で2分割し，迅速組織診（HE染色）に提出する。術後にはすべてのGNから永久組織診も行う。

⑤胃癌治療ガイドラインに沿った胃切除術を行う。術後，すべてのGN以外の郭清したリンパ節についてhilusを含む長軸方向の切片を作製し，リンパ節転移の検索を行う。リンパ節の固定標本の病理結果とGN迅速組織診の結果を比較検討する。

2. SNNS研究会による多施設共同研究における手技

SNNS研究会標準手技プロトコール作成委員会による多施設共同研究「胃癌におけるセンチネルリンパ節を指標としたリンパ節転移診断に関する臨床試験」は，RI法を基準とした胃癌におけるSNを指標としたリンパ節転移診断能を検証する臨床試験でprimary endpointは転移検出感度（リンパ節郭清の結果で所属リンパ節に少なくとも1個以上のリンパ節に転移が認められた症例のうちSNに転移を有した症例の割合）である。JCOG0302との相違点として，早期胃癌に加えて一部の進行胃癌（cT2）を対象とすること，トレーサー併用（放射性同位元素標識コロイドは必須）であること，術野サンプリングに加えて郭清終了時のバックテーブルでの再検索で検出されたものすべてを含めてSNとすること，術中迅速病理診断を原則とするが最終的リンパ節転移診断は永久標本での判定であること，30例以上の経験を持つ12施設に限定したものであること，などが挙げられる（**表1**）。SNNS研究会が行ったアンケート調査から，ラーニングカーブとして30例を要するとみられたことをふまえ，手技慣れを前提にSN conceptが胃癌においても成立するかをみることを主眼としており，術中迅速病理診断およびラーニングカーブの影響を受けにくいように設定されている。しかしながら，SN同定およびこれを指標としたリンパ節転移診断が切除郭清前に限定されていないため，臨床応用にはさらなる検証が求められる。

①手術前日，SN検索時の放射能が概ね11.1 MBq（0.3 mCi）となるように調整した

表 1　JCOG および SNNS 研究会による多施設共同研究の比較

	JCOG	SNNS 研究会
Primary endpoint	偽陰性割合（術中迅速病理診断）	転移検出感度
対象	sT1N0	cT1-2N0
トレーサーの種類（注入法）	ICG（開腹下に漿膜側から注入）	^{99m}Tc スズコロイド（手術前日に内視鏡で粘膜下層に注入），1% isosulfan blue（術中内視鏡で粘膜下層に注入）
同定・摘出法	術中ピックアップ（時間規定あり）	術野サンプリングしたものに加えて郭清終了時のバックテーブルでの再検索で検出されたものを含む
転移検索法	術中迅速病理診断	術中迅速診断を原則とするが最終的転移診断は永久標本判定
登録方法	術中登録	術前日までの前登録
参加施設	30 施設（手技慣れ各 5 施設）	30 例以上の経験を持つ 12 施設

^{99m}Tc スズコロイドを，内視鏡を用いて病変周囲粘膜下層に注入する。1 カ所 0.5 m*l* で 4 カ所への注入を原則とする。

②原則として術中に RI 法の補助として色素を併用した SN サンプリングを行う。胃大網動・静脈の外側で大網を切離して網嚢を開放し，リンパ流観察に適した状況を整え，1% isosulfan blue（Lymphazurin）を，内視鏡を用いて病変周囲粘膜下層に注入する。1 カ所 0.5 m*l* で 4 カ所への注入を原則とする。

③原則として RI 取り込みを認めるリンパ節を hot node（HN）とし，最終的な HN 判定は，術野サンプリングに加えて，郭清終了時のバックテーブルにおいて判定したものを併せて SN とする。色素法における同定はピックアップ法あるいは basin 法のいずれかで行い，20 分後までの間に青染されたリンパ節を blue node（BN）として摘出するが，basin 法では領域切除した lymphatic basin をバックテーブルで検索して摘出したものも BN とする。

④原則として同定した SN について最大割面の HE 染色による迅速組織診を行う。

⑤胃癌治療ガイドラインに沿った胃切除術を行う。最終的リンパ節転移診断は，リンパ節最大割面永久標本の HE 染色により診断する。

胃癌における SN concept が注目されるようになり 5 年以上が経過しているが[6)10)]，いまだ悪性黒色腫や乳癌の領域のように日常診療に用いられる現状ではない。すなわち，胃癌における SN concept は，多施設共同研究によりその妥当性が検証されている段階であり，日常診療として安易に臨床応用すべき状況にはない。両試験には検証点の相違があることに留意すべきだが，いずれも SN concept の胃癌治療への応用の可能性を検証する重要な試験であり，その結果が注目される。

文　献

1) 宮代　勲ほか：センチネルリンパ節の概念は消化器癌の外科治療を変えるか？変えるとする立場から．Front Gastroenterol 6 : 116-120, 2001
2) Nieweg OE et al : The definition of a sentinel node. Ann Surg Oncol 8 : 538-541, 2001
3) Cimmino VM et al : Allergic reactions to isosulfan blue during sentinel node biopsy-a common event. Surgery 130 : 439-442, 2001
4) 高山　敏ほか：Indocyanine green のリンパ系着色剤としての有用性．応用薬理 19 : 603-614, 1980

5) Gotoda T et al : Incidence of lymph node metastasis from early gastric cancer : estimation with a large number of cases at two large centers. Gastric Cancer 3 : 219-225, 2000
6) Hiratsuka M et al : Application of sentinel node biopsy to gastric cancer surgery. Surgery 129 : 335-340, 2001
7) 平塚正弘ほか：胃癌のセンチネルリンパ節の検出．消化器外科 23 : 1633-1638, 2000
8) 三輪晃一ほか：リンパ区域郭清を伴う早期胃がんの機能温存縮小手術．日外会誌 106 : 280-285, 2005
9) Ichikura T et al : Individualized surgery for early gastric cancer guided by sentinel node biopsy. Surgery 139 : 501-507, 2006
10) Kitagawa Y et al : The role of the sentinel lymph node in gastrointestinal cancer. Surg Clin North Am 80 : 1799-1809, 2000

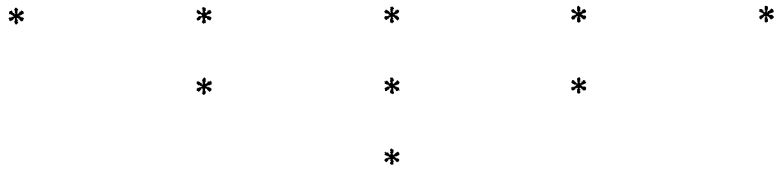

Ann Surg Oncol (2009) 16:1721
DOI 10.1245/s10434-009-0438-0

Annals of
SURGICAL ONCOLOGY
OFFICIAL JOURNAL OF THE SOCIETY OF SURGICAL ONCOLOGY

LETTER TO THE EDITOR

Reply: High Sensitivity of Indocyanine Green Fluorescence Imaging in Detection of Sentinel Node

TO THE EDITOR,

The argument by Takahashi et al. has been discussed in our article.[1] The following is our brief response.

Kitai et al. noted that the sensitivity of fluorescence spectroscopy is greater than that of absorption spectroscopy.[2] They also reported that it was possible to detect fluorescence with an indocyanine green (ICG) solution embedded 10 mm deep in a material that has optical properties like that of human tissue. In comparison, infrared rays can penetrate fatty tissues only to a depth of 3 mm. The difference could be critical in sentinel node detection. In this context, Ishikawa et al. reported an obese patient with a false-negative sentinel node when the infrared ray electronic endoscopy system was used.[3]

We reported that the ICG fluorescence imaging system was sensitive in both intraoperative ICG injection and ICG injection 1 day before surgery. We have argued that, similar to the radio-guided method, one advantage of preoperative tracer injection is that it eliminates the time-consuming intraoperative endoscopy, but has the disadvantage of loss of real-time tracing.[1]

An astral lamp, but not an ordinary light lamp, influences the ICG fluorescence imaging system. Therefore, surgery can be continued under an ordinary light lamp, which should not interfere with the ICG fluorescence imaging system. Furthermore, the light emitted by the laparoscope into the peritoneal cavity does not influence the ICG fluorescence imaging system. Laparoscopic exploration or surgery can be conducted under such an environment.

The laparoscopic system described in our report is not available commercially.[1] We have completed a preliminary study with a newly developed prototype system for laparoscopic surgery and are preparing a new report on its use in laparoscopic surgery.

Isao Miyashiro, MD
Department of Surgery, Osaka Medical Center for Cancer and Cardiovascular Diseases, 1-3-3 Nakamichi, Higashinari-ku, Osaka 537-8511, Japan
e-mail: miyashir@biken.osaka-u.ac.jp

Published Online: 21 March 2009

REFERENCES

1. Miyashiro I, Miyoshi N, Hiratsuka M, et al. Detection of sentinel node in gastric cancer surgery by indocyanine green fluorescence imaging: comparison with infrared imaging. *Ann Surg Oncol.* 2008;15:1640–3.
2. Kitai T, Inomoto T, Miwa M, et al. Fluorescence navigation with indocyanine green for detecting sentinel lymph nodes in breast cancer. *Breast Cancer.* 2005;12:211–5.
3. Ishikawa K, Yasuda K, Shiromizu A, et al. Laparoscopic sentinel node navigation achieved by infrared ray electronic endoscopy system in patients with gastric cancer. *Surg Endosc.* 2007;21:1131–4.

【ワンポイント・アドバイス】

胃癌におけるセンチネルリンパ節

宮代 勲 [大阪府立成人病センター消化器外科]

■腫瘍からのリンパ流を直接受けるリンパ節

腫瘍からのリンパ流を直接受けるリンパ節であるセンチネルリンパ節 sentinel node（SN）を同定することが可能であり，かつそこにリンパ節転移が認められなければ，SN以外のリンパ節には転移がないとして治療できるのではないか？ このコンセプトは，症例ごとにリンパ節転移有無を知るためのより確実・合理的な適応決定法として，悪性黒色腫や乳癌などの領域で臨床応用されている．

■リンパ節転移陰性を精度高く診断する指標

理論的には，リンパ節転移の可能性が非常に低い，もしくはなければ，後遺症を生じ得る胃切除やリンパ節郭清を予防的に行う意味はないと考えられるが，術前診断で得られた所見を過去のデータと照合することによりリンパ節転移がないであろう症例を割り出す現在の適応決定法では，根治性を保つために適応を厳しくせざるを得ない．リンパ節転移陰性を精度高く診断する指標の確立こそがブレークスルーとなる．根治性を損なうことなくリンパ節郭清を省略できれば，機能温存術式，腹腔鏡手術，内視鏡治療などへ展開できる．

■同定には適切なトレーサー注入が不可欠

SNの同定には適切なトレーサー注入が不可欠である．原発巣に近接して周囲を取り囲むように注入することが重要と考えられ，高度の線維化を伴う病変ではより注意を要する．トレーサーとしてradioisotope（RI）を用いる方法[1]は，放射線被曝，機器・試薬の取り扱いの煩雑さなどを伴い，取り扱いの容易な色素を用いる方法[2]は，経時的変化に弱い．色素のうち，isosulfan blue（Lymphazurin™）は日本で未承認であり，ショックを引き起こす可能性が低いとはいえない．異なる用途ではあるものの広く臨床で使用されているindocyanine green（ICG）は，リンパ系着色剤としての有用性が知られ，蛍光や赤外イメージングによる視認性向上の工夫も報告されている[3]．

■精度の高い術中迅速診断が求められる

SNの同定・摘出法には，pick up法やbasin法がある．また，basinではなくstationでの提唱もある．数個のリンパ節生検のみで転移診断を行うpick up法と異なり，basin法は支配動脈に伴走して5流域に分けられる胃のリンパ流のうち1～2流域を郭清するものである．もし，現行のリンパ節郭清を限られたリンパ流域のみの郭清に置換できるのであれば，nodeとしてのSNを同定・診断する必要はなく，lymphatic flowをみればよいことになるが，リンパ節郭清省略を目的とするSNコンセプトとの整合性が問われる．

SNコンセプトをリンパ節郭清省略に臨床応用するには，胃切除前にリンパ節転移陰性を診断する必要があり，精度の高い術中迅速診断が求められる．病理部門の理解と協力が不可欠といえる．

■多施設共同研究による妥当性の検証

早期胃癌のリンパ節転移は少なく，妥当性検証には方法論を統一した多数例での検討を要する．日本臨床腫瘍研究グループJapan Clinical Oncology Group（JCOG）とSentinel Node Navigation Surgery（SNNS）研究会による二つの多施設共同研究が行われた．

JCOG胃がん外科グループによる「早期胃癌におけるセンチネルリンパ節生検の妥当性に関する研究（JCOG0302）」は，早期胃癌患者に対して，ICGを用いて同定されたgreen node（GN）をSNとみなし，GNの術中迅速病理診断でリンパ節転移陰性の場合にリンパ節郭清を行わないことの妥当性を評価することを目的とし，primary endpointは偽陰性割合（GN迅速病理診断転移陰性例/組織学的リンパ節転移陽性例）である．現時点で臨床応用した場合にどうなるかをみる設定であるため，SNコンセプトの妥当性のみならず，術中迅速病理診断およびラーニングカーブの問題などが包含されている点に留意すべきである．実際，偽陰性例の検討からこれらの問題が予想以上に大きいことが示唆されている．

SNNS研究会標準手技プロトコール作成委員会

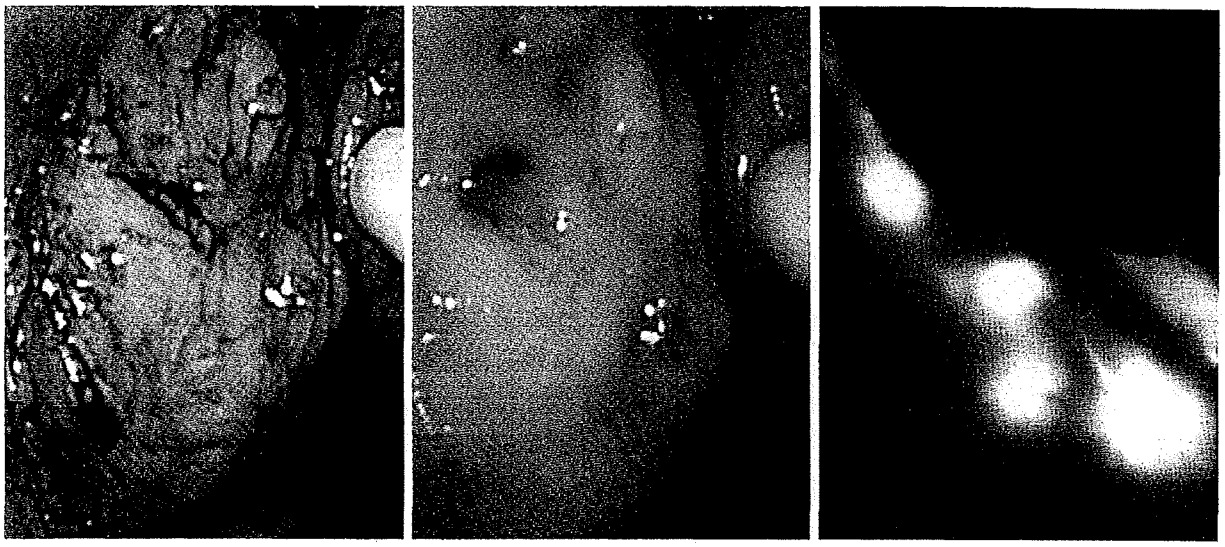

[図1] ICGをトレーサーとした蛍光や赤外イメージングによる視認性向上の工夫

ICGの緑色だけ（左図）では同定しにくいリンパ節も，赤外イメージング（中央図）により認識しやすくなり，蛍光イメージング（右図）では4個と視認できる．（文献3）より引用一部改変）

による「胃癌におけるセンチネルリンパ節を指標としたリンパ節転移診断に関する臨床試験」は，RI法を基準とした胃癌におけるSNを指標としたリンパ節転移診断能を検証する試験でprimary endpointは転移検出感度（リンパ節郭清の結果で所属リンパ節に少なくとも1個以上のリンパ節に転移が認められた症例のうちSNに転移を有した症例の割合）である．例えば，同定・診断を切除前に限定していないなど，実臨床に応用するには課題が残るが，SNコンセプト自体をみる観点から，術中迅速病理診断やラーニングカーブの影響を受けにくいように設定されている．

胃癌におけるSNコンセプトは多施設共同研究によりその妥当性が検証されている段階であり，日常診療として安易に臨床応用すべき状況にはない．両試験には検証点の違いがあることに留意すべきであるが，いずれもSNコンセプトの胃癌治療への応用の可能性を検証する重要な試験であり，今後の展開が注目される．

文献

1）Kitagawa, Y et al：The role of the sentinel lymph node in gastrointestinal cancer. Surg Clin North Am 80：1799-1809, 2000

2）Hiratsuka, M et al：Application of sentinel node biopsy to gastric cancer surgery. Surgery 129：335-340, 2001

3）Miyashiro, I et al：Detection of sentinel node in gastric cancer surgery by indocyanine green fluorescence imaging：comparison with infrared imaging. Ann Surg Oncol 15：1640-1643, 2008

V 胃癌手術の Knack & Pitfalls

VI 腹腔鏡下手術の Knack & Pitfalls

［検印省略］

Knack & Pitfalls
胃外科の要点と盲点

定価（本体 18,000 円＋税）

2003年1月26日　第1版第1刷発行
2009年7月17日　第2版第1刷発行

監　修＝幕内雅敏
編　集＝荒井邦佳
発行者＝浅井宏祐
発行所＝株式会社 文光堂

〒113-0033 東京都文京区本郷7-2-7
電話　東京（03）3813-5478（営業）
東京（03）3813-5411（編集）

印刷所＝真興社

Printed in Japan

ISBN978-4-8306-2326-4

乱丁・落丁の際はお取り替えいたします

Identification of a predictive gene expression signature of cervical lymph node metastasis in oral squamous cell carcinoma

Su Tien Nguyen,[1,3] Shogo Hasegawa,[2] Hitoshi Tsuda,[4] Hirofumi Tomioka,[2] Masaru Ushijima,[5] Masaki Noda,[3,7] Ken Omura[2,3] and Yoshio Miki[1,3,6,8]

[1]Department of Molecular Genetics, Medical Research Institute, [2]Oral and Maxillofacial Surgery, Department of Oral Restitution, Division of Oral Health Sciences, Graduate School and [3]21st Century Center of Excellent Program for Frontier Research on Molecular, Destruction and Reconstruction of Tooth and Bone, Tokyo Medical and Dental University, 1-5-45 Yushima, Bunkyo-ku, Tokyo 113-8510; [4]Department of Basic Pathology, National Defense Medical College, 3-2, Namiki, Tokorozawa, Saitama 359-1192; [5]Bioinformatics Group, Genome Center, and [6]Department of Genetic Diagnosis, Cancer Institute, Japanese Foundation for Cancer Research, 3-10-6, Ariake Koto-ku, Tokyo 135-8550; [7]Department of Molecular Pharmacology, Medical Research Institute, Tokyo Medical and Dental University, 2-3-10, Kanda-Surugadai, Chiyoda-ku, Tokyo 101-0062

(Received December 12, 2006/Revised January 20, 2007/Accepted January 27, 2007/Online publication March 19, 2007)

An accurate assessment of the cervical lymph node metastasis status in oral cavity cancer not only helps predict the prognosis of patients, but also helps surgeons to perform the appropriate treatment. We investigated the utilization of microarray technology focusing on the differences in gene expression profiles between primary tumors of oral squamous cell carcinoma that had metastasized to cervical lymph nodes and those that had not metastasized in the hope of finding new biomarkers to serve for diagnosis and treatment of oral cavity cancer. To design this experiment, we prepared two groups: the learning case group with 30 patients and the test case group with 13 patients. All tissue samples were performed using laser captured microdissection to yield cancer cells, and RNA was isolated from purified cancer cells. To identify a predictive gene expression signature, the different gene expressions between the two groups with and without metastasis in the learning case ($n = 30$) were analyzed, and the 85 genes expressed differentially were selected. Subsequently, to construct a more accurate prediction model, we further selected the genes with a high power for prediction from the 85 genes using the AdaBoost algorithm. The eight candidate genes, *DCTD, IL-15, THBD, GSDML, SH3GL3, PTHLH, RP5-1022P6* and *C9orf46*, were selected to achieve the minimum error rate. Quantitative reverse transcription–polymerase chain reaction was carried out to validate the selected genes. From these statistical methods, the prediction model was constructed including the eight genes and this model was evaluated by using the test case group. The results in 12 of 13 cases (~92.3%) were predicted correctly. (*Cancer Sci* 2007; 98: 740–746)

In 2005, 335 870 Japanese people died from cancer. Of these, 5679 people had oral cavity cancer (http:www.mhlw.go.jp/toukei/saikin/hw/jinkou/suikei05/index.html) and the major cause of death by cancer was metastasis. An accurate assessment of the cervical lymph node metastasis status in oral cavity cancer not only helps predict the prognosis of patients, but also helps surgeons to carry out the appropriate treatment. When the disease is localized, surgical procedures can be used to remove the tumor in its entirety. For patients who are diagnosed clinically as cervical lymph node metastasis-positive (N+), a surgical procedure, known as radical neck dissection (RND), is used to remove all lymph node groups from levels I, II, III, IV and V, which involves the sacrifice of the internal jugular vein, sternocleidomastoid muscle and spinal accessory nerve.

The clinical diagnostic procedure for clinical staging of cervical lymph nodes is carried out by clinical examination of the neck region or by ultrasound, computed tomography and magnetic resonance imaging. But the sensitivity of these methods is still limited. Post-operative histological examination shows that approximately 30% of clinically diagnosed metastasis-negative (N0) patients have metastasis-positive lymph nodes in the neck,[1] and 10–20% of clinically diagnosed metastasis-positive (N+) patients turn out to be metastasis-free. Due to the fact that the false-negative rate is high in clinically diagnosed metastasis-negative (N0) patients, most surgeons would not like to select a 'wait and watch' policy, because it may allow metastasis to spread further. Thus, the surgeons usually carry out a supraomohyoid neck dissection (SOHND) to remove lymph nodes at levels I, II and III to screen for metastasis. Although SOHND is not as stringent as RND and the technique of neck dissection has been perfected over the last century, surgeons still face minor and major complications during the surgical procedure,[2] also sequelae such as chronic pain and limitation of shoulder movement due to a weak trapezius muscle.

Metastasis is a very complicated process. To metastasize, the cancer cells must break away from the tumor, increase their mobility and move through the extracellular matrix. Next they must invade the lymph vessels and grow in the lymph nodes or invade blood vessels and travel in the circulatory system. They then can pass through the vessel walls into surrounding tissue (distant metastasis). We think that the original genes controlling this process and the gene products of this process may be used as predictive markers of cervical lymph node metastasis. In the present study, microarray technology was used to investigate the differences in gene expression profiles between primary tumors of oral squamous cell carcinoma (OSCC) that metastasized to cervical lymph nodes and those that did not metastasize, in an effort to find new biomarkers that will provide more accurate diagnosis and more appropriate treatment for OSCC.

Materials and Methods

Tumor samples. All of the primary oral cancer specimens were obtained from anonymous patients who were previously untreated at the Faculty of Dentistry, Tokyo Medical and Dental University and were defined as squamous cell carcinoma of the oral cavity by histopathology. Informed consent was obtained from all of the patients. All clinical materials were approved by the ethics committee. The samples were embedded using Tissue-Tek OCT Compound (Sakura Finetek USA) and stored at −80°C until use. These samples were grouped into metastasis group and non-metastasis group based on clinical diagnosis and histological

[8]To whom correspondence should be addressed. E-mail: miki.mgen@mri.tmd.ac.jp

doi: 10.1111/j.1349-7006.2007.00454.x

Table 1. Clinical and histological characteristics of individual patients

Case	Sex	Age (years)	Primary site	TN	Differentiation	Prediction score
Learning case						
1	M	56	Lower gingival	T2N0	Moderately	−0.791
2	M	62	Buccal mucosa	T1N0	Well	−0.032
3	M	55	Upper gingival	T2N0	Well	−0.780
4	F	66	Tongue	T2N0	Moderately	−0.309
5	M	72	Hard palate	T1N0	Moderately	−0.481
6	M	58	Mouth floor	T2N0	Well	−0.716
7	M	80	Tongue	T2N0	Well	−0.564
8	M	30	Tongue	T2N0	Well	−0.609
9	F	81	retromolar trigone	T1N0	Well	−0.507
10	F	60	Tongue	T2N0	Well	−0.264
11	M	59	Tongue	T3N0	Moderately	−0.481
12	M	68	retromolar trigone	T2N0	Moderately	−0.428
13	M	54	Tongue	T1N0	Well	−0.534
14	M	56	Upper gingival	T2N0	Well	−0.303
15	M	43	Tongue	T2N0	Moderately	−0.716
16	M	46	Tongue	T2N0	Well	−0.564
17	M	58	Tongue	T2N0	Well	−0.282
18	F	64	Lower gingival	T4aN1	Well	0.348
19	M	66	Tongue	T1N2b	Moderately	0.411
20	M	77	Lower gingival	T2N2b	Poor	0.577
21	F	74	Buccal mucosa	T2N1	Moderately	0.780
22	M	78	Lower gingival	T2N1	Well	0.499
23	M	71	Buccal mucosa	T3N2b	Poor	0.499
24	M	71	Lower gingival	T3N2b	Well	0.564
25	M	61	Tongue	T2N2c	Moderately	0.318
26	M	60	Lower gingival	T4N2b	Moderately	1.000
27	M	57	Upper gingival	T4aN1	Poor	0.571
28	M	70	Tongue	T3N1	Moderately	0.592
29	M	52	Lower gingival	T4aN2b	Moderately	0.817
30	M	37	Tongue	T2N3	Poor	0.292
Test case						
1	M	66	Lower gingival	T2N0	Well	−0.318
2	F	66	Upper gingival	T2N0	Moderately	−0.288
3	M	73	Tongue	T2N0	Poor	−0.507
4	M	32	Tongue	T3N0	Moderately	−0.260
5	M	58	Mouth floor	T3N0	Moderately	−0.053
6	M	72	Lower gingival	T2N0	Well	−0.165
7	M	66	Mouth floor	T3N1	Moderately	0.162
8	M	68	Lower gingival	T4aN2b	Moderately	0.214
9	F	54	Tongue	T2N2b	Moderately	0.329
10	M	59	Mouth floor	T4N1	Moderately	0.115
11	M	67	Mouth floor	T4N1	Well	0.143
12	M	60	Tongue	T4N2c	Moderately	0.164
13	M	53	Tongue	T2N2b	Moderately	−0.228

T1, tumor ≤2 cm in greatest dimension; T2, tumor >2 cm but ≤4 cm in greatest dimension; T3, tumor >4 cm in greatest dimension; T4, (lip) tumor invades through cortical bone, inferior alveolar nerve, floor of mouth, or skin of face (i.e. chin or nose); T4a, (oral cavity) tumor invades adjacent structures (e.g. through cortical bone, into deep [extrinsic] muscle of tongue [genioglossus, hyoglossus, palatoglossus, and styloglossus], maxillary sinus, and skin of face); T4b, tumor invades masticator space, pterygoid plates, or skull base and/or encases internal carotid artery; N0, no regional lymph node metastasis; N1, metastasis in a single ipsilateral lymph node, ≤3 cm in greatest dimension; N2, metastasis in a single ipsilateral lymph node, >3 cm but ≤6 cm in greatest dimension, or in multiple ipsilateral lymph nodes, ≤6 cm in greatest dimension, or in bilateral or contralateral lymph nodes, ≤6 cm in greatest dimension; N2a, metastasis in a single ipsilateral lymph node >3 cm but ≤6 cm in dimension; N2b, metastasis in multiple ipsilateral lymph nodes, ≤6 m in greatest dimension; N2c, metastasis in bilateral or contralateral lymph nodes, ≤6 cm in greatest dimension; N3, metastasis in a lymph node >6 cm in greatest dimension.

examination. For the learning case, 30 samples were prepared (Table 1) including 13 samples from patients who were found to be N+ in the cervical lymph node and 17 samples from patients who were found to be N0 in the cervical lymph node. Those that remained metastasis-free were monitored for at least 1 year after the primary tumor was removed. (The primary tumors were surgically removed between April 2004 and October 2005.) For the test case, 13 samples were prepared (Table 1) including seven samples found to be N+ in the cervical lymph node and six samples found to be N0 in the cervical lymph node. Those remaining metastasis-free were monitored for at least 6 months after the primary tumor was removed. (The primary tumors were surgically removed between November 2005 and April 2006.) To determine the technical reproducibility, we prepared eight samples from the learning case for a replicate experiment.

Laser captured microdissection. All primary tumor specimens were cut into 9-μm sections at −20°C using a LEICA cryostat model 3050S. The sections were mounted on a special slide for use in laser captured microdissection (LCM) and immediately placed at −80°C before use. First, the sections were fixed in cold

ethanol for 3 min. They were then were washed in dionised water for 30 s, stained with hematoxylin for 40 s, and again washed in dionised water for 30 s. The sections were dried by cold wind for 2 or 3 min before the LCM. Squamous cell carcinomas were obtained accurately from the hematoxylin-stained tissue sections by LCM.

RNA isolation and quality assessment. Total RNA was extracted from the harvested cells using the RNeasy Micro Kit of Qiagen, and the concentration was measured using a NanoDrop ND-100 Spectrophotometer. All RNA was run with RNA 6000 Pico LabChip kits on the Agilent 2100 Bioanalyzer to analyze the quality of total RNA. The total RNA quality was assessed by RNA integrity number (RIN) value,[3,4] and the samples with RIN values below 5[5] were not used for the next step.

cRNA amplification and biotin labeling. Total RNA (100 ng) of each sample was used for starting the protocol of Two-Cycle cDNA Synthesis and labeling of cRNA, following the recommendations of Affymetrix.[6] The yield of biotin-labeled cRNA was measured using a NanoDrop ND-100 Spectrophotometer and the quality was analyzed using an Agilent 2100 Bioanalyzer. We removed samples with a yield less than 40 μg or with a median size of biotin-labeled cRNA fragments less than 500 bp.

Microarray production. The Human Genome U133 Plus 2.0 array was purchased from the Affymetrix company in Japan. The array comprised 1 300 000 distinct oligonucleotides and featured over 47 000 transcripts and variants, including approximately 39 000 of the best-characterized human genes.

Cocktail solution and microarray hybridization. Before making a cocktail solution, we used 20 μg of biotin-labeled cRNA and broke down the full length to 35–200 base fragments. Then, we used 15 μg of broken cRNA to make the cocktail solution, and the solution was put into GeneChip HG U133 plus 2 and hybridized for 16 h at 45°C. After hybridization, the arrays were washed and stained using Fluidic station 450 with protocol EukGE-WS2v5_450 and the arrays were scanned using the Affymetrix GeneChip Scaner 3000.

Statistical analysis. After scanning, the fluorescence intensity was measured using Affymetrix Microarray Suite 5.0 software, and the array was removed if it had a report with a scale factor larger than 6, 3′/5′ β-actin larger than 35 or 3′/5′ glyceraldehyde-3-phosphate dehydrogenase larger than 7. At low-level analysis, the arrays were imported into the RMAExpress software (http://rmaexpress.bmbolstad.com) to perform normalization using the RMA algorithm[7,8] and computing expression levels, because the RMA algorithm gave the most reproducible results and showed the highest correlation coefficients with real-time polymerase chain reaction data.[9,10] After the expression levels were calculated, the array data were imported into DNA-Chip analysis software (http://www.dchip.org) for high-level analysis. Gene filtering was carried out using the variation across samples criteria ($0.3 <$ standard deviation/mean < 100). For group comparison, two-group *t*-tests were used with a threshold of $P < 0.04$, absolute value of the difference in mean expression between two groups (Δ) > 100 intensity units and a fold change in mean expression >1.5 and <0.66. The 85 genes (Table 2) were selected. After selecting 85 genes that showed a difference in expression levels between the two groups, we again extracted from the 85 genes with software using the Adaboost algorithm.[11] The software was able to autoselect the best gene combination for separating the metastasis group from the non-metastasis group with the lowest cross validation (CV) error rate. Eight genes (Table 3) were extracted with a higher power for prediction, and were used to evaluate 13 samples from the test case.

Quantitative reverse transcription–polymerase chain reaction analysis. Quantitative reverse transcription–polymerase chain reaction (RT-PCR)[12] was to validate the results of eight meaningfully expressed genes from the analyzed microarray array data. For each sample, 100 ng of original total RNA was used to synthesize the first strand of cDNA by reverse transcriptase using oligo dT primer following the protocol recommended by Invitrogen (Superscript III First-Strand Synthesis System for RT-PCR). Primer sets for quantitative RT-PCR (Table 4) were designed

Table 2. The 85 genes related to lymph node metastasis

Accession no.	Gene symbol	Description	Fold change	*P*-value
Downregulated genes in the metastasis group				
NM_000597	*IGFBP2*	Insulin-like growth factor binding protein 2, 36 kDa	−6.81	0.004005
NM_002276	*KRT19*	Keratin 19	−5.78	0.028855
BG401568	*SLC16A9*	Solute carrier family 16 (monocarboxylic acid transporters), member 9	−3.54	0.000823
NM_001387	*DPYSL3*	Dihydropyrimidinase-like 3	−3.33	0.035334
NM_016140	*CGI-38*	Brain specific protein /// brain specific protein	−2.49	0.019781
NM_001823	*CKB*	Creatine kinase, brain	−2.42	0.006229
AF288571	*LEF1*	Lymphoid enhancer-binding factor 1	−2.35	0.033874
NM_002820	*PTHLH*	Parathyroid hormone-like hormone	−2.34	0.02038
AW451197		CDNA clone IMAGE:5278089	−2.32	0.035398
AI278995		Predicted: *Homo sapiens* similar to B230208J24Rik protein (LOC201501), mRNA	−2.24	0.01941
M31157	*PTHLH*	Parathyroid hormone-like hormone	−2.16	0.038689
NM_003027	*SH3GL3*	SH3-domain GRB2-like 3	−2.15	0.029178
AL567411	*CDK5R1*	Cyclin-dependent kinase 5, regulatory subunit 1 (p35)	−2.13	0.011045
BG434174		Stoned B-like factor	−2.11	0.023189
AI522132		Hypothetical protein LOC115749	−2.04	0.038373
BC005961	*PTHLH*	Parathyroid hormone-like hormone /// parathyroid hormone-like hormone	−2.00	0.022891
NM_001759	*CCND2*	Cyclin D2	−1.98	0.018311
BG290193	*ZNF703*	Zinc finger protein 703	−1.93	0.037675
AI189753	*TM4SF1*	Transmembrane 4 L six family member 1	−1.92	0.011249
AA143793	*RAB11FIP1*	RAB11 family interacting protein 1 (class I)	−1.89	0.013964
BF111651	*PPAPDC1B*	Phosphatidic acid phosphatase type 2 domain containing 1B	−1.89	0.03133
AL137763	*GRHL3*	Grainyhead-like 3 (Drosophila)	−1.89	0.035038
BC000408	*ACAT2*	Acetyl-Coenzyme A acetyltransferase 2 (acetoacetyl Coenzyme A thiolase)	−1.88	0.006495
AW026491	*CCND2*	Cyclin D2	−1.87	0.032209
AL137629	*KALRN*	Kalirin, RhoGEF kinase	−1.82	0.031132
BF514585	*SESN3*	Sestrin 3	−1.77	0.021875

doi: 10.1111/j.1349-7006.2007.00454.x

Table 2. *continued*

Accession no.	Gene symbol	Description	Fold change	*P*-value
M90657	*TM4SF1*	Transmembrane 4 L six family member 1	−1.76	0.011547
AI458128	*CBX6*	Chromobox homolog 6	−1.73	0.018388
BF680438	*LONRF1*	LON peptidase N-terminal domain and ring finger 1	−1.70	0.01133
AU154469	*SLC11A2*	Solute carrier family 11 (proton-coupled divalent metal ion transporters), member 2	−1.69	0.018722
BG165333	*CNKSR3*	CNKSR family member 3	−1.68	0.016795
AI654238	*B4GALNT3*	β1,4-*N*-acetylgalactosaminyltransferase-transferase-III	−1.63	0.018618
AI346835	*TM4SF1*	Transmembrane 4 L six family member 1	−1.52	0.006659
Upregulated genes in the metastasis group				
BE501952	*SATL1*	Spermidine/spermine N1-acetyl transferase-like 1	1.51	0.015987
AI809870	*SMYD2*	SET and MYND domain containing 2	1.54	0.003793
NM_017665	*ZCCHC10*	Zinc finger, CCHC domain containing 10	1.54	0.010698
BF214329		Mitochondrial fission regulator 1	1.56	0.008586
AI123233	*RANBP6*	RAN binding protein 6	1.58	0.0279
NM_016040	*TMED5*	Transmembrane emp24 protein transport domain containing 5	1.59	0.015651
NM_001889	*CRYZ*	Crystallin, zeta (quinone reductase)	1.59	0.012586
NM_013322	*SNX10*	Sorting nexin 10	1.59	0.028971
NM_024699	*ZFAND1*	Zinc finger, AN1-type domain 1	1.6	0.018314
U13700	*CASP1*	Caspase 1, apoptosis-related cysteine peptidase (interleukin 1, beta, convertase)	1.61	0.02315
AW157773	*ZFP62*	Zinc finger protein 62 homolog (mouse)	1.61	0.016554
NM_016283	*TAF9*	TAF9 RNA polymerase II, TATA box binding protein (TBP)-associated factor, 32 kDa	1.62	0.012154
BF439522	*MGC23909*	Hypothetical protein MGC23909	1.63	0.017789
NM_003187	*TAF9*	TAF9 RNA polymerase II, TATA box binding protein (TBP)-associated factor, 32 kDa	1.65	0.006175
NM_014873	*LPGAT1*	Lysophosphatidylglycerol acyltransferase 1	1.65	0.010458
AK001947	*RP5-1022P6.2*	Hypothetical protein KIAA1434	1.65	0.026428
NM_016576	*GMPR2*	Guanosine monophosphate reductase 2	1.66	0.039452
NM_024430	*PSTPIP2*	Proline-serine-threonine phosphatase interacting protein 2	1.67	0.016465
AW612657	*LYPLAL1*	Lysophospholipase-like 1	1.67	0.021165
L12723	*HSPA4*	Heat shock 70 kDa protein 4	1.69	0.006059
BC001025	*RCL1*	RNA terminal phosphate cyclase-like 1	1.71	0.007725
AI042152	*TncRNA*	Trophoblast-derived noncoding RNA	1.71	0.02217
AW962511	*FLJ22531*	Hypothetical protein FLJ22531	1.73	0.036123
AI634046	*CFLAR*	CASP8 and FADD-like apoptosis regulator	1.74	0.03599
AF183569	*ARTS-1*	Type 1 tumor necrosis factor receptor shedding aminopeptidase regulator	1.76	0.009405
AI805560	*ZMYM6*	Zinc finger, MYM-type 6	1.77	0.01367
AI347128	*IGBP1*	Immunoglobulin (CD79A) binding protein 1	1.77	0.001289
NM_002198	*IRF1*	Interferon regulatory factor 1	1.8	0.016707
NM_000361	*THBD*	Thrombomodulin	1.81	0.007352
NM_000361	*THBD*	Thrombomodulin	1.84	0.007352
NM_012485	*HMMR*	Hyaluronan-mediated motility receptor (RHAMM)	1.84	0.009623
BF735901	*NUDCD2*	NudC domain containing 2	1.86	0.00967
AL559202		Full-length cDNA clone CS0DF034YI03 of fetal brain of *Homo sapiens* (human)	1.86	0.009237
AW973232		gb:AW973232 /DB_XREF=gi:8163078 /DB_XREF=EST385330 /FEA=EST /CNT=5 /TID=Hs.293553.0 /TIER=ConsEnd /STK=0 /UG=Hs.293553 /UG_TITLE=ESTs	1.89	0.008534
NM_004120	*GBP2*	Guanylate binding protein 2, interferon-inducible /// guanylate binding protein 2, interferon-inducible	1.89	0.029524
U29343	*HMMR*	Hyaluronan-mediated motility receptor (RHAMM)	1.92	0.004741
AW119113	*THBD*	Thrombomodulin	1.92	0.010555
NM_018530	*GSDML*	Gasdermin-like	1.95	0.027119
NM_014349	*APOL3*	Apolipoprotein L, 3	1.95	0.018873
AI224133		Transcribed locus, weakly similar to XP_517454.1 PREDICTED: similar to hypothetical protein MGC45438 [Pan troglodytes]	1.96	0.039636
AI928035	*IRX2*	Iroquois homeobox protein 2	1.99	0.022852
NM_018465	*C9orf46*	Chromosome 9 open reading frame 46	1.99	0.014382
AW003140		mRNA; cDNA DKFZp686K1098 (from clone DKFZp686K1098)	2.04	0.025115
AW613387		Endothelial cell growth factor 1 (platelet-derived)	2.09	0.013803
NM_001657	*AREG*	Amphiregulin (schwannoma-derived growth factor)	2.10	0.013069
BC005254	*CLEC2B*	C-type lectin domain family 2, member B	2.11	0.024784
AI656493	*DCTD*	dCMP deaminase	2.17	0.004514
NM_005415	*SLC20A1*	Solute carrier family 20 (phosphate transporter), member 1	2.17	0.022575
NM_004815	*ARHGAP29*	Rho GTPase activating protein 29	2.27	0.009215
AA976354	*KIAA1618*	KIAA1618	2.61	0.017377
NM_000585	*IL15*	Interleukin 15	2.80	0.00711
AI539443	*STAT1*	Signal transducer and activator of transcription 1, 91 kDa	3.00	0.033578

Table 3. Genes selected for the prediction model

Accession	Gene symbol	Description	Fold change	*P*-value
AI656493	*DCTD*	dCMP deaminase	2.17	0.004514
NM_000585	*IL15*	Interleukin 15	2.80	0.00711
AW119113	*THBD*	Thrombomodulin	1.92	0.010555
NM_018530	*GSDML*	Gasdermin-like	1.92	0.027119
NM_003027	*SH3GL3*	SH3-domain GRB2-like 3	−2.15	0.029178
BC005961	*PTHLH*	Parathyroid hormone-like hormone	−2.00	0.022891
BE328402	*RP5-1022P6*	Hypothetical protein KIAA1434	1.92	0.020426
NM_018465	*C9orf46*	Chromosome 9 open reading frame 46	1.99	0.014382

Table 4. Primers for the genes used in real-time polymerase chain reaction

Gene symbol	Product size (bps)	Forward primer	Reverse primer
DCTD	113	ctgcgaggctcctgtttaat	aagcttttgactcggtctgc
IL15	103	acaaacatcactctgctgcttagac	ctgatccaaggtctgatcatcttct
THBD	105	agcacttgtgttgtctggtggt	tgtgcacacagagatagcatgaa
GSDML	149	tgaggcacgaattctctgtg	ggcagtgaggacagactggt
SH3GL3	103	gcttcctgtcctaaaagtcattggt	ctgaggaatataggccattcgttg
PTHLH	122	tgtggcttgtttatccttagctc	cttgccctaggttgtgaact
RP5-1022P6	104	caatgagctttgcacagtttga	tagtcccttagcttttgcctcttg
C9orf46	121	cttcctggtcccgattgttc	actcttttctgtttccagtatgtcctc
Actin	150	atgtggccgaggactttga	tgtgtggacttgggagagga

using PRIMER 3 software (http://www.genome.wi.mit.edu) and were synthesized by the Sigma Corporation. The PCR reaction was carried out using an ABI Prism 7900 Sequence Detection system with Power SYBR Green Master Mix (15 μL Power SYBR Green Master Mix, 0.3 μL with 5 μM of each primer, 5 μL cDNA, 9.4 μL water). For each sample, reactions were carried out in triplicate following the program: denaturation for 15 s at 95°C, and annealing and extension for 60 s at 60°C. Cumulative fluorescence was measured at the end of the extension phase of each cycle. Quantification was based on standard curves from serial dilution of human normal total RNA purchased from Stratagene Corporation. The results were normalized by to actin, and then compared with the microarray data of eight genes.

Results

To identify a predictive gene expression signature, 30 primary tumor samples (learning case group) located in the oral cavity region were analyzed. These included 13 samples from individuals who were found postoperatively to have metastasis in the lymph node of the neck, and 17 samples from individuals who were found postoperatively to have no metastasis in the lymph node of the neck and who remained metastasis-free when monitored for at least 1 year after primary tumor removal. The cancer cells of the tumor were obtained by LEM technology. Total RNA was isolated and its quality checked. We removed samples with RIN values below 5. At first, technical reproducibility was determined using eight samples from the training case. The technical replicates of the same two-sample comparison showed a high Pearson correlation coefficient. The lowest Pearson correlation coefficient was 0.9433 (Supplementary Fig. S1). This result indicated that the technical reproducibility of gene expression was high. To analyze the results of 30 primary tumors samples, two-group *t*-tests were used with a threshold of $P < 0.04$ and an absolute value of the difference in mean expression between the two groups (Δ) > 100 intensity units, with fold change in mean expression >1.5 and <0.66. The 85 genes expressed differentially between the two patient groups with and without cervical lymph node metastasis were selected (Table 2), including 33 genes that were downregulated and 52 genes that were upregulated in the metastasis group. Next, hierarchical clustering was carried out using 85 genes from the 30 samples by Pearson's correlation distance metric and average linkage (Fig. 1). Two major cluster branches were created. One major cluster included 16 non-metastasis samples and the other included 13 metastasis samples and one non-metastasis sample (missed clustering). Subsequently, to construct a more accurate and practical prediction model using a smaller number of genes, we selected further the genes with a high power for prediction from the 85 genes using AdaBoost algorithm.[11] In the AdaBoost algorithm, the optimal gene and its weight are determined in each boosting step, and the prediction model is constructed by weighted voting of the selected genes. We performed 1000 replicates of five-fold cross validation for the learning cases. Eight candidate genes (*DCTD*, *IL-15*, *THBD*, *GSDML*, *SH3GL3*, *PTHLH*, *RP5-1022P6* and *C9orf46*) were selected (Table 3), which achieved the minimum error rate. Next a prediction score was established for each sample (Table 1). Prediction scores have a value from −1 to 1, and the borderline is 0. A positive score indicates cervical lymph node metastasis, whereas a negative score indicates that the sample is metastasis-free. In the learning case, all 13 metastasis samples had positive scores and all 17 non-metastasis samples had negative scores (Fig. 2A). Microarray is an excellent tool that can analyze the expression of tens of thousands of genes. However it has some problems with accuracy and universal use. For the prediction system with high accuracy, verification that we could accurately analyze gene expression using this method was required. Thus, to confirm the prediction results, quantitative RT-PCR of the selected eight genes was carried out and normalized to actin before being compared by microarray data. The Pearson correlation values of the eight genes between microarray data and quantitative RT-PCR data were calculated and revealed to be over 0.73 (Table 5), showing a high correlation between microarray data and quantitative RT-PCR data in this study. We evaluated the prediction model by using the test case group. A prediction score was calculated for each sample using the prediction model constructed in this study (Fig. 2B). Six non-metastasis samples and six of the seven metastasis samples (~92.3%) were predicted correctly by the prediction model. Only one case (~7.7%) was a failure by this prediction model (circled in red in Fig. 2B).

doi: 10.1111/j.1349-7006.2007.00454.x

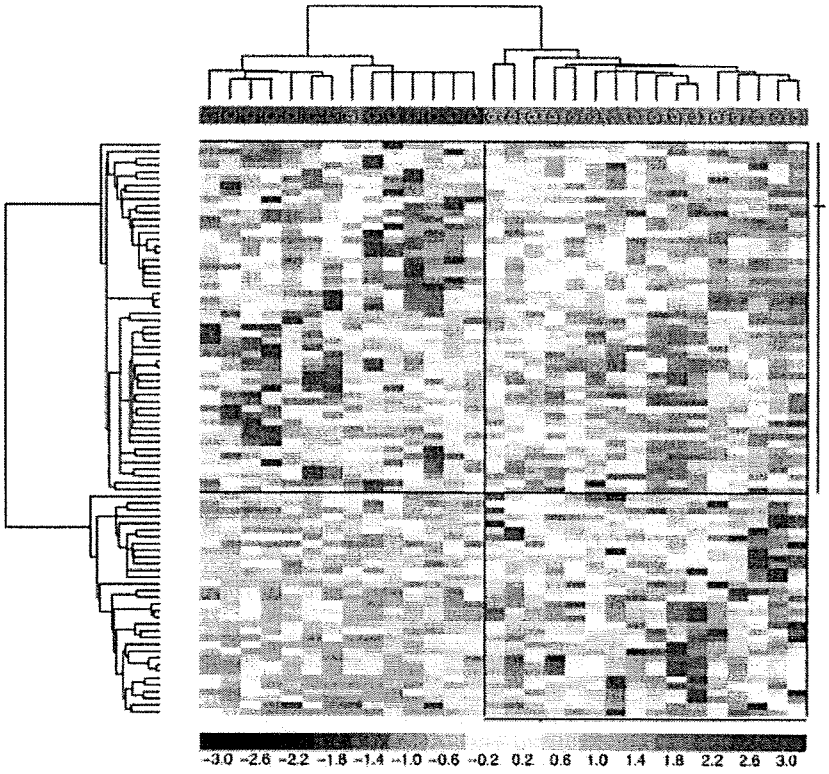

Fig. 1. Hierarchical clustering for 85 genes from 30 samples, including 13 metastasis samples (shown by pink color +) and 17 non-metastasis samples (shown by green color –). Red color shows that the gene is upregulated and blue color shows that the gene is downregulated. Two major cluster branches were created. One major cluster included 16 non-metastasis samples and the other one included 13 metastasis samples and one non-metastasis sample (missed clustering).

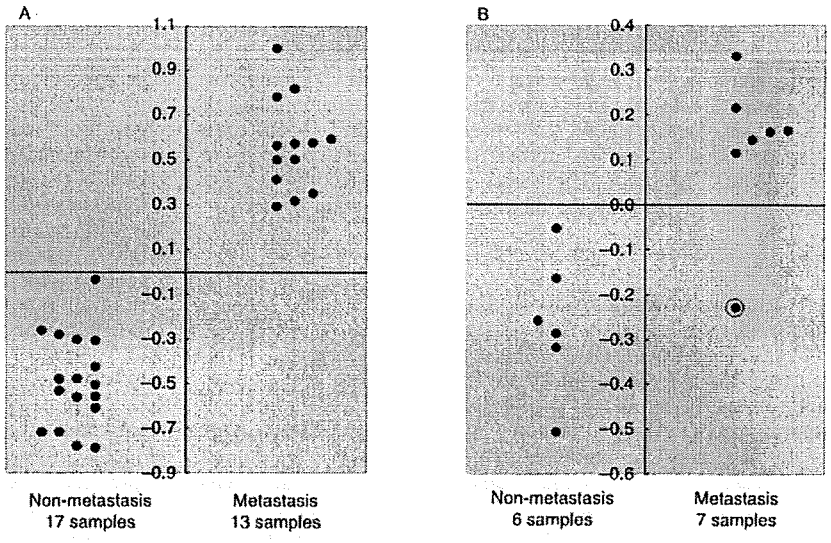

Fig. 2. The samples were rank-ordered by their score (determined by the Adaboost algorithm). A vertical line shows the total discriminant score. The samples with negative score indicated that the tumors were free of lymph node metastasis. The samples with positive scores indicated that the tumors metastasized to the cervical lymph node. (A) The prediction result of learning cases. All of the 17 samples in the non-metastasis group were negative and all of the 13 samples in the metastasis group were positive. (B) The prediction results of test cases. The six samples in the non-metastasis group were negative. Six of seven samples in the metastasis group were positive and one was negative (failure sample, circled in red).

Table 5. Pearson correlation of expression values between microarray data and real-time polymerase chain reaction data of the eight genes

Gene symbol	Pearson correlation	*P*-value
DCTD	0.796	2.46×10^{-7}
IL15	0.739	4.74×10^{-6}
THBD	0.753	2.49×10^{-6}
GSDML	0.868	1.06×10^{-9}
SH3GL3	0.911	6.86×10^{-12}
PTHLH	0.852	4.69×10^{-9}
RP5-1022P6	0.768	1.18×10^{-6}
C9orf46	0.742	4.05×10^{-6}

Discussion

At present, the methods for diagnosing the status of lymph node metastasis in oral cavity cancer are not accurate. Thus, two opinions were formed about the treatment of individual clinically diagnosed oral cavity cancer cases that are cervical lymph node metastasis-free. The first is the 'neck dissection' policy and the other is the 'wait and watch' policy. However, neither policy provides appropriate treatment for the disease. Because the neck dissection policy can cause pain, discomfort and in some cases leads to complications (such as chronic pain and shoulder palsy), it is important to ascertain whether a patient really is metastasis-free. The alternative 'wait and watch' policy may

allow an overlooked metastasis to spread widely for the patient who has micrometastasis. The goal of our study is to devise a novel diagnostic system that may improve the diagnosis of N status in oral cavity cancer. The results in 12 of 13 cases (~92.3%) were predicted correctly. Only one case (~7.7%) was a failure by this prediction model. The misjudged metastasis case using our prediction model was a 53-year-old man with moderately differentiated tongue squamous cell carcinoma. It is very difficult to discuss why the case missed, because we could not find any relationship between clinicopathological features of the patient and the score. In this study we would like to say that quantitative RT-PCR data should not be use for this prediction model system. The data could not be predicted accurately. The reason was that the prediction score from microarray data were normalized by RMA algorithm, but the quantitative RT-PCR data were normalized to actin; therefore the gene expression value of each gene by quantitative RT-PCR data differs from the microarray data.

Of the eight genes identified, *IL-15* is of particular interest. IL-15 is a cytokine that regulates T and natural killer cell activation and proliferation. Studies on mice suggest that IL-15 may increase the expression of apoptosis inhibitor. A recent study has reported that IL-15 expression has been shown to play an important role in cell proliferation, invasion and metastasis of human colorectal cancer.[13,14] In the present study, we observed IL-15 overexpression in the metastasis group (fold change [FC]: 2.8, $P < 0.00711$; Pearson correlation between microarray data and real-time PCR, 0.739). This showed that IL-15 may also play a role in the metastasis of oral squamous cell carcinoma. Further study is required to learn more about the roles of IL-15 in the metastasis of OSCC.

A second interesting gene is *PTHLH*. The protein encoded by this gene is a member of the parathyroid hormone family. This hormone regulates endochondral bone development and epithelial–mesenchymal interactions during formation of the mammary glands and teeth. Some articles have reported that PTHLH may play a role in metastasis of breast cancer and prostate cancer cell lines by upregulation.[15,16] But in our results, *PTHLH* was upregulated in the non-metastasis group and downregulated in the metastasis group (FC: −2, $P < 0.022891$; Pearson correlation between array data and real-time PCR, 0.852). It is difficult to explain why, but it may be that the *PTHLH* mechanism is different *in vitro* compared with *in vivo*, or it may be that the role of PTHLH in each type of cells is different. It could also be that cancer cells produce PTHLH to prompt cancer cell migration and invasion, but when the metastasis process is finished PTHLH is no longer necessary and so was downregulated in the metastasis group. Further study may clarify the role of *PTHLH* in OSCC.

The novel diagnosis system using gene sets may be applied in diagnosis of the disease. Further, the system may be also applied for other diseases in the future.

Acknowledgments

Many thanks to Drs Takashi Shimoji, Koichi Nagasaki, Kiyotsugu Yoshida, Masaru Uekusa and Fumiyuki Uematsu for helpful discussion during the preparation of this article. We also thank Professor Marie Cosgrove for having checked the English language of this paper.

References

1 Jones AS, Phillips DE, Helliwell TR, Roland NJ. Occult node metastases in head and neck squamous carcinoma. *Eur Arch Otorhinolaryngol* 1993; **250**: 446–9.
2 Genden EM, Ferlito A, Shaha AR *et al.* Complications of neck dissection. *Acta Otolaryngol* 2003; **123**: 795–801.
3 Mueller O, Lightfoot S, Schroeder A. RNA integrity number (RIN) standardization of RNA quality control. Agilent Application Note, May 1 2004. Publication no. 5989-1165EN. Available from URL: http://www.gene-quantification.de/RIN.pdf
4 Imbeaud S, Graudens E, Boulanger V *et al.* Towards standardization of RNA quality assessment using user-independent classifiers of microcapillary electrophoresis traces. *Nucleic Acids Res* 2005; **33**: e56.
5 Lee J, Hever A, Willhite D, Zlotnik A, Hevezi P. Effects of RNA degradation on gene expression analysis of human postmortem tissues. *FASEB J* 2005; **19**: 1356–8.
6 Technical note. GeneChip Eukaryotic Small Sample Target Labeling Assay Version II. Available from URL: http://genomics.msu.edu/RTSF/small_sample_labeling.pdf
7 Irizarry RA, Bolstad BM, Collin F, Cope LM, Hobbs B, Speed TP. Summaries of Affymetrix GeneChip probe level data. *Nucleic Acids Res* 2003; **31**: e15.
8 Li J, Spletter ML, Johnson JA. Dissecting tBHQ induced ARE-driven gene expression through long and short oligonucleotide arrays. *Physiol Genomics* 2005; **21**: 43–58.
9 Irizarry RA, Hobbs B, Collin F *et al.* Exploration, normalization, and summaries of high density oligonucleotide array probe level data. *Biostatistics* 2003; **4**: 249–64.
10 Millenaar FF, Okyere J, May ST, van Zanten M, Voesenek LA, Peeters AJ. How to decide? Different methods of calculating gene expression from short oligonucleotide array data will give different results. *BMC Bioinformatics* 2006; **7**: 137.
11 Freund Y, Schapire RE. A short introduction to boosting. *J. Japan. Soc. Artif. Intel.* 1999; **14**: 771–80.
12 Ginzinger DG. Gene quantification using real-time quantitative PCR: an emerging technology hits the mainstream. *Exp Hematol* 2002; **30**: 503–12.
13 Kuniyasu H, Ohmori H, Sasaki T *et al.* Production of interleukin 15 by human colon cancer cells is associated with induction of mucosal hyperplasia, angiogenesis, and metastasis. *Clin Cancer Res* 2003; **9**: 4802–10.
14 Kuniyasu H, Oue N, Nakae D *et al.* Interleukin-15 expression is associated with malignant potential in colon cancer cells. *Pathobiology* 2001; **69**: 86–95.
15 Shen X, Qian L, Falzon M. PTH-related protein enhances MCF-7 breast cancer cell adhesion, migration, and invasion via an intracrine pathway. *Exp Cell Res* 2004; **294**: 420–33.
16 Shen X, Falzon M. PTH-related protein modulates PC-3 prostate cancer cell adhesion and integrin subunit profile. *Mol Cell Endocrinol* 2003; **199**: 165–77.

Supplementary Material

The following supplementary material is available for this article:

Fig. S1. Replicated experiment of eight samples. The technical replicates of the same two-sample comparison, showed a high Pearson correlation coefficient.

This material is available as part of the online article from:

http://www.blackwell-synergy.com/doi/abs/10.1111/j.1349-7006.2007.00454.x

<http://www.blackwell-synergy.com/doi/abs/10.1111/j.1349-7006.2007.00454.x>

(This link will take you to the article abstract).

Please note: Blackwell Publishing are not responsible for the content or functionality of any supplementary materials supplied by the authors. Any queries (other than missing material) should be directed to the corresponding author for the article.

doi: 10.1111/j.1349-7006.2007.00454.x

One-step Nucleic Acid Amplification for Intraoperative Detection of Lymph Node Metastasis in Breast Cancer Patients

Masahiko Tsujimoto,[1] Kadzuki Nakabayashi,[14] Katsuhide Yoshidome,[2] Tomoyo Kaneko,[8] Takuji Iwase,[9] Futoshi Akiyama,[8] Yo Kato,[8] Hitoshi Tsuda,[12] Shigeto Ueda,[13] Kazuhiko Sato,[13] Yasuhiro Tamaki,[3] Shinzaburo Noguchi,[3] Tatsuki R. Kataoka,[4] Hiromu Nakajima,[5] Yoshifumi Komoike,[6] Hideo Inaji,[6] Koichiro Tsugawa,[11] Koyu Suzuki,[10] Seigo Nakamura,[11] Motonari Daitoh,[14] Yasuhiro Otomo,[14] and Nariaki Matsuura[7]

Abstract

Purpose: Detection of sentinel lymph node (SLN) metastasis in breast cancer patients has conventionally been determined by intraoperative histopathologic examination of frozen sections followed by definitive postoperative examination of permanent sections. The purpose of this study is to develop a more efficient method for intraoperative detection of lymph node metastasis.

Experimental Design: Cutoff values to distinguish macrometastasis, micrometastasis, and nonmetastasis were determined by measuring cytokeratin 19 (CK19) mRNA in histopathologically positive and negative lymph nodes using one-step nucleic acid amplification (OSNA). In an intraoperative clinical study involving six facilities, 325 lymph nodes (101 patients), including 81 SLNs, were divided into four blocks. Alternate blocks were used for the OSNA assay with CK19 mRNA, and the remaining blocks were used for H&E and CK19 immunohistochemistry–based three-level histopathologic examination. The results from the two methods were then compared.

Results: We established CK19 mRNA cutoff values of 2.5×10^2 and 5×10^3 copies/μL. In the clinical study, an overall concordance rate between the OSNA assay and the three-level histopathology was 98.2%. Similar results were obtained with 81 SLNs. The OSNA assay discriminated macrometastasis from micrometastasis. No false positive was observed in the OSNA assay of 144 histopathologically negative lymph nodes from pN0 patients, indicating an extremely low false positive for the OSNA assay.

Conclusion: The OSNA assay of half of a lymph node provided results similar to those of three-level histopathology. Clinical results indicate that the OSNA assay provides a useful intraoperative detection method of lymph node metastasis in breast cancer patients.

Authors' Affiliations: Departments of [1]Pathology and [2]Surgery, Osaka Police Hospital, [3]Department of Breast and Endocrine Surgery, Osaka University Graduate School of Medicine, Departments of [4]Pathology, [5]Clinical Laboratory, and [6]Surgery, Osaka Medical Center for Cancer and Cardiovascular Diseases, and [7]Department of Molecular Pathology, Osaka University Graduate School of Medicine and Health Science, Osaka, Japan; Departments of [8]Pathology and [9]Breast Surgery, Cancer Institute of the Japanese Foundation for Cancer Research, and Departments of [10]Pathology and [11]Breast Surgical Oncology, St. Luke's International Hospital, Tokyo, Japan; Departments of [12]Pathology II and [13]Surgery I, National Defense Medical College, Saitama, Japan; and [14]Central Research Laboratories, Sysmex Corp., Kobe, Japan

Received 10/16/06; revised 4/3/07; accepted 5/15/07.

The costs of publication of this article were defrayed in part by the payment of page charges. This article must therefore be hereby marked *advertisement* in accordance with 18 U.S.C. Section 1734 solely to indicate this fact.

Note: Supplementary data for this article are available at Clinical Cancer Research Online (http://clincancerres.aacrjournals.org/).

M. Tsujimoto and K. Nakabayashi contributed equally to this work.

Requests for reprints: Nariaki Matsuura, Department of Molecular Pathology, Graduate School of Medicine and Health Science, Osaka University, 1-7 Yamadaoka, Suita, Osaka 565-0817, Japan. E-mail: matsuura@sahs.med.osaka-u.ac.jp.

doi:10.1158/1078-0432.CCR-06-2512

Sentinel lymph node (SLN) biopsy has recently become a standard surgical procedure in the treatment of breast cancer patients (1–10). This procedure can predict metastasis to the regional lymph nodes with high accuracy and avoids unnecessary removal of axillary lymph nodes and subsequent morbidity associated with axially clearance in node negative breast cancer patients.

SLN metastasis is generally detected by conventional means including the intraoperative H&E-based histopathologic examination of frozen section(s) or cytologic observation of touch-imprints, followed by definitive postoperative histopathologic examination of permanent sections (2, 7–9). However, the sensitivity of these intraoperative methods is not high. Many investigators have reported that the intraoperative H&E-based histopathologic examination has a false-negative rate of 5% to 52% (reviewed in ref. 11). Furthermore, these methods provide subjective rather than objective results, which may differ from one pathologist to another (12). On the other hand, the definitive postoperative histopathologic examination generally requires 5 to 10 days for assessment. If an accurate

intraoperative method is developed, the test results can allow for completion of axillary node dissection during surgery and avoidance of a second surgical procedure in patients with positive SLNs, thereby reducing patient distress and, finally, saving hospital costs (2, 13, 14). Accordingly, the development of a precise and objective intraoperative method for the detection of lymph node metastasis is important for increasing the efficiency of breast cancer surgery (10, 13–18).

To overcome the shortcomings of the present histopathologic methods, molecular biological methods based on quantitative reverse transcription-PCR (QRT-PCR) have been studied extensively for the detection of lymph node metastasis in breast cancer patients (12, 19–25). A QRT-PCR assay with multiple mRNA markers including cytokeratin 19 (CK19), trefoil factor 3 (p1B), epithelial glycoprotein 2 (EGP2), and small breast epithelial mucin (SBEM) resulted in a 10% upstaging compared with the routine histopathologic analysis (22). It was also reported that a QRT-PCR assay using mRNA markers of CK19 and mammaglobin 1 (MGB1) was almost as accurate (94.1% sensitivity and 98.6% specificity) as that of the conventional histopathologic examination (12). This study included a discussion of the drawbacks of using a single marker like CK19 mRNA for which the QRT-PCR may include the concomitant amplification of CK19 pseudogenes within genomic DNA, giving false positive results.

We recently developed a one-step nucleic acid amplification (OSNA) assay (Fig. 1A), which consists of solubilization of a lymph node followed by reverse-transcription loop-mediated isothermal amplification (RT-LAMP) of a target mRNA (26, 27). The RT-LAMP reaction is a new method of gene amplification, and its application has been reported previously (28–32). The OSNA method is characterized by the quantitative measurement of a target mRNA in a metastatic lymph node, a brief reaction time for the OSNA process, a high specificity for the target mRNA, and an absence of genomic DNA amplification.

In this paper, we report an efficient intraoperative detection method for lymph node metastasis in breast cancer patients using the OSNA assay with CK19 mRNA as a target marker. The results of a multicenter clinical study including 325 lymph nodes are discussed from the viewpoint of the usefulness of the OSNA assay as an intraoperative detection method.

Materials and Methods

Lymph nodes for selection of mRNA markers and determination of cutoff values. Lymph nodes, which were used to select mRNA markers and determine cutoff values, were obtained from Osaka Police Hospital with the approval of its internal review board. Lymph nodes were stored at -80°C until use.

QRT-PCR. QRT-PCR was carried out by ABI Prism 7700 sequence detector. RNA was purified from a lymph node lysate using RNeasy Mini Kit (Qiagen), and then purified RNA was subjected to one-step RT-PCR with QuantiTect SYBR Green (Qiagen) according to the manufacturer's instructions. The sequences of the forward and reverse primers used are shown in Supplementary Table S1. The primers were designed by Primer Express Version 2.0 software (ABI).

Selection of mRNA maker. Forty-five candidate mRNA markers, selected as being specific to breast cancer tissue, were identified from the public EST database (33). The performance of these mRNA markers was evaluated with QRT-PCR using a mixture of four histopathologically positive and four negative lymph nodes. The results were summarized as C_t (threshold cycle) values for each mRNA marker (see Supplementary Table S2). The selected markers, KRT19 (CK19), CEACAM5 (CEA), forkhead box A1 (FOXA1), SAM-pointed domain containing ETS transcription factor (SPDEF), tumor-associated calcium signal transducer 2 (TACSTD-2), mucin 1 (MUC1), and MGB1, were further evaluated with QRT-PCR using 11 histopathologically positive and 15 negative lymph nodes from 26 patients.

RT-LAMP reaction of CK19 mRNA. The RT-LAMP reaction was carried out according to the Notomi's method (26, 27). The human CK19 mRNA was synthesized by *in vitro* transcription from cloned cDNA.

A 2-μL sample of human CK19 mRNA in a lysis buffer containing 200 mmol/L glycine-HCl, 20% DMSO, and 5% Brij35 (pH 3.5) was added to 23 μL of solution consisting of 3.5 μmol/L each of the forward inner (CK19FA) and reverse primer (CK19RA), 0.2 μmol/L each of forward outer (CK19F3) and reverse primer (CK19R3), 2.6 μmol/L each of forward loop (CK19LPF) and reverse primer (CK19LPR), 0.9 mmol/L deoxynucleotide triphosphates, 54.3 mmol/L Tris-HCl, 10.8 mmol/L KCl, 10.8 mmol/L $(NH_4)_2SO_4$, 5.4 mmol/L $MgSO_4$, 0.1% Triton X-100, 5.4 mmol/L DTT, 2.5 units avian myeloblastosis virus reverse transcriptase (Promega), 18 units Bst DNA Polymerase (New England Biolabs), and 25 units RNasin Plus (Promega). Each reaction mixture contained three pairs of primer sets including the loop primer (27). The sequences of the human CK19 primers were designed as amplicons spanning exon junction regions between CK19 exons 1 and 2 and were

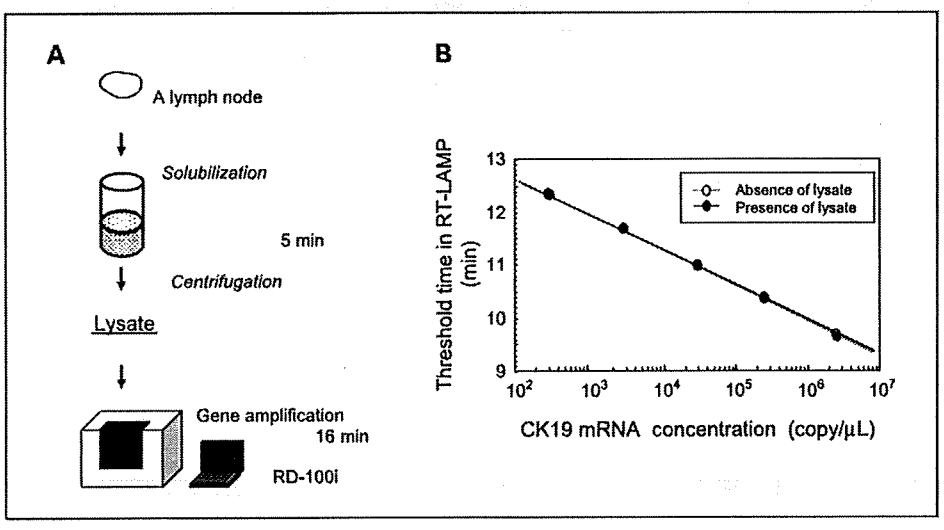

Fig. 1. OSNA assay. *A*, schematic diagram of the OSNA procedure. *B*, standard curve of human CK19 mRNA measured by RD-100i in the presence and absence of lymph node lysate. A histopathologically negative lymph node (600 mg) was homogenized in 4 mL of lysis buffer. A 180-μL sample of the lymph node lysate was added to 20 μL of human CK19 mRNA in the lysis buffer. The final concentration of human CK19 mRNA was adjusted to 2.5×10^6, 2.5×10^5, 2.5×10^4, 2.5×10^3, and 2.5×10^2 copies/μL. A 2-μL sample of each was subjected to the RT-LAMP reaction under the same conditions described in Materials and Methods.

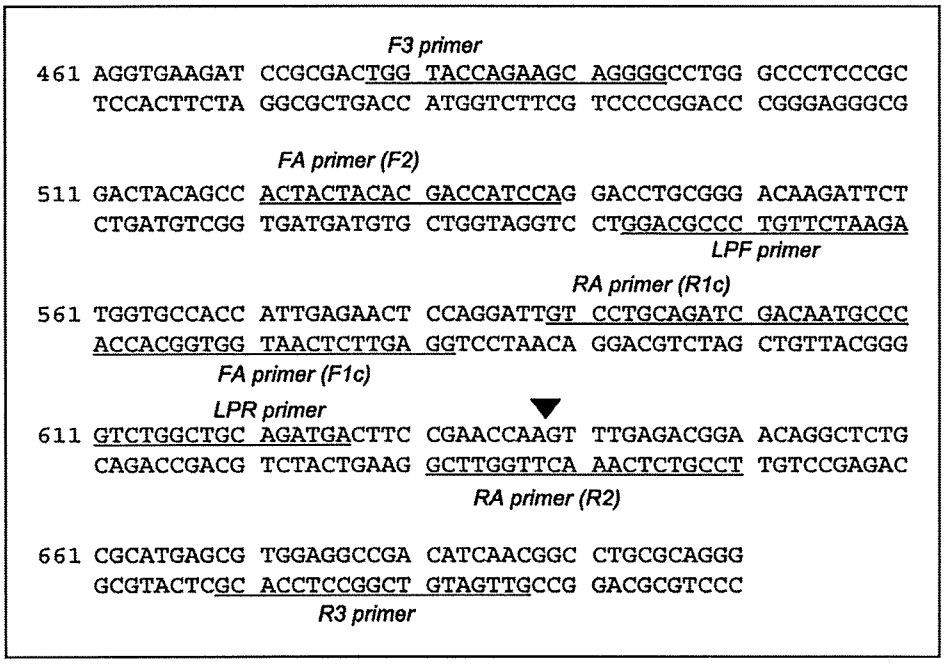

Fig. 2. A schematic representation of primer placement along the CK19 cDNA sequence. The CK19 cDNA sequence (NM.002276) and the sequence of the primers for the CK19 RT-LAMP are shown. The location on CK19 cDNA where each primer-set binds is underlined. The sequence of the inner primer (FA and RA) consists of discontinuous two different regions, F1c and F2 (or R1c and R2), to create the stem structure during the RT-LAMP reaction. The exon junction between exons 2 and 3 is included in the sequence of the R2 region in the RA primer (*arrowhead*).

furthermore designed as mismatch sequences of the CK19a and CK19b pseudogenes (GenBank accession number M33101 and U85961) using Probe Wizard (RNAture). Primer sequences were 5′-GGAGTTCT-CAATGGTGGCACCAACTACTACACGACCATCCA-3′ (CK19FA), 5′-GTCCTGCAGATCGACAACGCCTCCGTCTCAAACTTGGTTCG-3′ (CK19RA), 5′-TGGTACCAGAAGCAGGGG-3′ (CK19F3), 5′-GTTGATGTCGGCCTCCACG-3′ (CK19R3), 5′-AGAATCTTGTCCCG-CAGG-3′ (CK19LPF), and 5′-CGTCTGGCTGCAGATGA-3′ (CK19LPR). The sequence of each primer and its placement along the CK19 cDNA sequence are shown in Fig. 2.

The RT-LAMP reaction with CK19 mRNA was carried out in a gene amplification detector, RD-100i (Sysmex). Mori et al. (34, 35) reported that PPi, which is produced in the course of the RT-LAMP reaction, binds to magnesium ion to result in magnesium PPi. The amount of magnesium PPi increases with the passage of the reaction. Magnesium PPi has a low solubility in aqueous solution and precipitates when its concentration reaches saturation. The amplification of CK19 mRNA was monitored by measuring the turbidity of the reaction mixture at 6-s intervals. The threshold time was defined as the time at which the turbidity exceeded 0.1.

OSNA assay. A schematic diagram of the OSNA assay with CK19 mRNA is shown in Fig. 1A. A histopathologically negative lymph node (≤600 mg) was homogenized in 4 mL of the above lysis buffer for 90 s on ice using a Physicotron Warring blender with an NS-4 shaft (MicroTec Nichion). The homogenate was centrifuged at 10,000 × *g* for 1 min at room temperature. A 2-μL sample of the supernatant (lysate) was subjected to the RT-LAMP reaction under the same conditions as above. CK19 mRNA copy number was determined based on the standard curve using a known quantity of human CK19 mRNA.

Effect of lymph node size on the OSNA assay. A histopathologically negative lymph node (130 mg) was homogenized in 4 mL of lysis buffer under the same conditions as above. A 180-μL sample of lymph node lysate was added to 20 μL of human CK19 mRNA in the lysis buffer. The final concentration of human CK19 mRNA was adjusted to 2.5×10^5 and 2.5×10^3 copies/μL. About 2 μL of each sample was subjected to the RT-LAMP reaction under the same conditions described above. Each sample was assayed in duplicate. Other histopathologically negative lymph nodes (214, 354, and 428 mg) were treated under the same conditions as above.

Amplification of genomic DNA by the OSNA assay. Genomic DNA was extracted from histopathologically positive lymph nodes using QIAamp DNA Mini Kit (Qiagen) according to the manufacturer's instructions. Purified genomic DNA (100 ng) was subjected to the OSNA assay using the CK19 primers described above.

Protocol for determining the cutoff values. A cutoff value (*L*) for the OSNA assay between metastatic positive and negative lymph nodes was determined using 106 lymph nodes (42 histopathologically negative lymph nodes from pN0 patients, 42 histopathologically negative lymph nodes from pN1-3 patients, and 22 histopathologically positive lymph nodes) from 30 patients (24 ductal carcinomas, 5 special types, and 1 ductal carcinoma *in situ*). As shown in Fig. 3A, the central part of one quarter of a frozen lymph node (40-600 mg) of 1 mm thickness was dissected out. Four levels (i, ii, iii, and iv) were used as permanent slices for the histopathologic examination with H&E and immunohisto-chemistry using anti-CK19 antibody (DAKO) as shown in Fig. 3A.

Histopathologically positive lymph nodes were defined as those that were positive at any of four levels (i, ii, iii, and iv). Histopathologically negative lymph nodes were defined as those that were negative in all four levels. Blocks a and c were used for the OSNA assay. A cutoff value was determined by statistical analysis of the copy numbers obtained by the OSNA assay of the histopathologically negative lymph nodes from pN0 patients.

According to the tumor-node-metastasis (TNM) classification of the Unio Internationale Contra Cancrum (Italian) sixth and the American Joint Committee on Cancer sixth editions (36), macrometastasis is defined as having metastatic foci of ≥2 mm in the long axis. In the OSNA assay, macrometastasis is assumed as having the amount of CK19 mRNA expression in 2^3 mm^3 of metastatic foci. Based on this assumption, we estimated a cutoff value (*H*) for CK19 mRNA between macrometastasis and micrometastasis as follows. Nine frozen histo-pathologically positive lymph nodes from nine breast cancer patients (8 ductal and 1 lobular carcinomas) were used to estimate the amount of CK19 mRNA expression in 2^3 mm^3 of metastatic foci (Table 1). A frozen lymph node was serially sectioned at 10-μm intervals. Each slice was first examined with CK19 immunohistochemistry–based histo-pathologic examination to measure the area of metastatic foci and then with RT-LAMP to measure CK19 mRNA expression. The procedure is detailed in Fig. 3B.

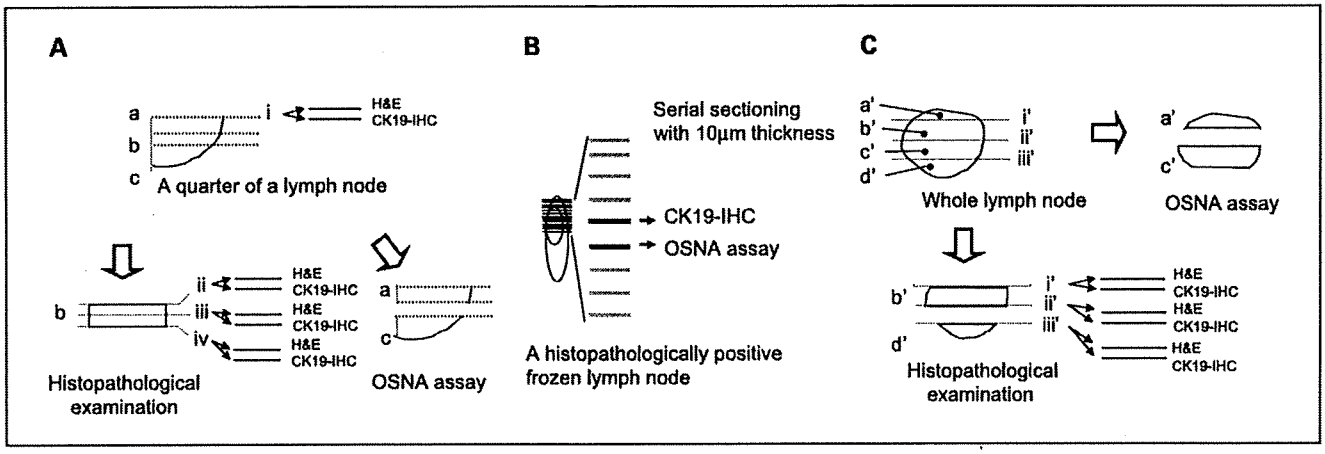

Fig. 3. Protocols. *A*, protocol for determining a cutoff value for micrometastasis and nonmetastasis. *B*, protocol for determining the cutoff value between macrometastasis and micrometastasis. Serial frozen sections taken at 10-μm intervals were prepared from histopathologically positive lymph nodes. One of two consecutive frozen sections was subjected to CK19 immunohistochemistry (CK19-IHC)–based histopathologic examination to measure the area of metastatic foci, and then the volume of the metastatic foci was calculated by multiplying the area by the thickness of the slice. The adjacent section was subjected to the OSNA assay. The expression level of CK19 mRNA in 2^3 mm^3 was estimated based on the correlation between the volume of metastatic foci and CK19 mRNA expression. *C*, clinical study protocol.

In the OSNA assay, an amount of CK19 mRNA expression less than the cutoff value was indicated as (-), an amount of CK19 mRNA expression between the cutoff values *L* and *H* was indicated as (+), and an amount of CK19 mRNA expression greater than the cutoff value *H* was indicated as (++).

Clinical study protocol. An intraoperative clinical study was conducted from February 2005 to July 2005 at six facilities other than Sysmex Central Research Laboratories. A total of 325 fresh lymph nodes (101 patients), including 81 SLNs (49 patients), were used with the approval of the internal review board at each facility. The clinicopathologic characteristics of patients are shown in Table 2. A large percent of patients had stages I A/B and II A/B. The majority of patients had a nodal status of pN0 and pN1. About 80% of patients had invasive ductal carcinoma.

A fresh lymph node with a short axis of 4 to 12 mm was divided into four blocks at 1- or 2-mm intervals using our original cutting device (Fig. 3C and 4). Blocks a' and c' were used for the OSNA assay. Two slices were cut from each of the three cutting surfaces (i', ii', and iii'), as shown in Fig. 3C, and used for the permanent three-level histopathologic examination with H&E and CK19 immunohistochemistry.

In the histopathologic examination, macrometastasis and micrometastasis were defined according to the TNM classification of the Unio Internationale Contra Cancrum sixth and American Joint Committee on Cancer sixth editions (36). All samples for histopathologic examination were examined by three third-party pathologists. Conflicting results were settled consensually. The performance of the OSNA assay was compared with the three-level histopathology.

The OSNA assay analyzed different blocks from those used in the three-level histopathologic examination. Therefore, in this protocol, the sensitivity and specificity of the OSNA assay could not be calculated based on the histopathologic results. For this reason, we evaluated the performance of the OSNA assay as a concordance rate with the three-level histopathologic examination.

In the case of lymph nodes from pN0 patients, blocks b' and d' were further sliced at 0.2-mm intervals, followed by staining each alternate slice with H&E and CK19 immunohistochemistry (Fig. 3C). A total of 144 lymph nodes, in which neither macrometastasis nor micrometastasis were observed in the above serial sectioning examination, were used for the false positive study of the OSNA assay.

When discordance between the OSNA assay and the three-level histopathologic examination occurred, a histopathologic analysis of blocks b' and d' was repeated. All slides for the histopathologic examination were examined and evaluated by three third-party pathologists. All results of histopathologic examinations were finally determined by a study group comprised of representatives from the different facilities.

Analysis of discordant cases. In the analysis of discordant cases, QRT-PCR and CK19 Western blot analysis of the lysates were carried out. QRT-PCR was carried out with TaqMan RT-PCR. RNA was purified from lymph node lysates using RNeasy Mini Kit (Qiagen), and then the purified RNA was subjected to TaqMan one-step RT-PCR universal master mix (ABI) according to the manufacturer's instructions. The sequences of the forward and reverse primers designed for human CK19 were 5'-CAGATCGAAGGCCTGAAGGA-3' and 5'-CTTGGCCCCT-CAGCGTACT-3', respectively. The sequence of the TaqMan probe, containing a fluorescent reporter dye (FAM) at the 5' end and a fluorescent quencher dye (TAMRA) at the 3' end, was 5'-FAM-GCCTACCTGAA-GAAGAACCATGAGGAGGAA-TAMRA-3'. The primers and TaqMan probe were obtained from Applied Biosystems (ABI). All QRT-PCR reactions were done in duplicate.

In the CK19 Western blot analysis, lysate (20 μL) was added to 10 μL of loading buffer containing 150 mmol/L Tris-HCl, 300 mmol/L DTT, 6% SDS, 0.3% bromophenol blue, and 30% glycerol. The solution was boiled and electrophoresed on a polyacrylamide gel in the presence of

Table 1. CK19 mRNA expression in 2^3 mm^3 of metastatic foci

Case	Histology	CK19 mRNA (copy/μL)
1	Ductal carcinoma	2.3×10^4
2	Ductal carcinoma	1.1×10^4
3	Ductal carcinoma	4.7×10^3
4	Ductal carcinoma	5.0×10^4
5	Ductal carcinoma	1.0×10^4
6	Lobular carcinoma	1.4×10^5
7	Ductal carcinoma	2.0×10^4
8	Ductal carcinoma	6.7×10^4
9	Ductal carcinoma	2.4×10^4
	Average	3.0×10^4

NOTE: CK19 mRNA expression in 2^3 mm^3 of metastatic foci was estimated on the basis of the examination of serial sections (Fig. 3B).